Effects of inlet velocity and steam-to-methanol ratio on the phenomena of process intensification in protruded millisecond microchannel reactors

Junjie Chen [a, b, *]

[a] Department of Mechanical and Aerospace Engineering, College of Engineering, University of California, Davis, California, 95616, United States

[b] Department of Energy and Power Engineering, School of Mechanical and Power Engineering, Henan Polytechnic University, Jiaozuo, Henan, 454000, P.R. China

* Corresponding author, E-mail address: junjiem@tom.com

Abstract

The present study focuses upon the physics of heat and mass transfer processes in a protruded millisecond microchannel reactor, wherein a steam reforming reaction is proceeding and protrusions are used to improve the transport processes involved. Parametric analysis of the reactor system is carried out using a three-dimensional numerical model that is sufficiently detailed to delineate the role of geometric features and operation conditions in reactor performance. Computational fluid dynamics analyses are performed under different sets of circumstances. In analysing the mechanisms involved in the intensified processes, account is taken of the factors that may influence the reactor performance. New insights into the physics of the processes are presented, with recommendations on how to optimize reactor design for better performance. The results indicate that the flow rates and feed compositions must be adjusted as needed to maximize production of hydrogen and minimize pressure drops. Protrusions are very effective in improving the transport processes involved without greatly impairing hydraulic performance. Methanol can be converted effectively to hydrogen due to the successive continuous interruptions in the presence of hemispherical protrusions. Necessary adjustments to the molar ratio of steam to methanol can be made to control the maximum reactor temperature within certain needed limits. Protrusions can be used to improve the conversion and productivity due to enhanced heat and mass transfer, as they behave as a baffle to direct flow of the reforming process flow stream.

Keywords: Process intensification; Methanol processors; Reforming reactions; Operation conditions; Periodic wakes; Efficient operation

1. Introduction

Continuous and efficient production of hydrogen from fuel in microchemical systems remains a major engineering design challenge. Significant improvements in hydrogen productivity, combined with the rising costs of fossil fuels, will contribute to the wider use of fuel cells. Traditionally, the important processes for hydrogen production are autothermal reforming [1], partial oxidation [2], and especially steam reforming [3, 4]. The high energy density of alcohols [5, 6], ammonia [7, 8], and hydrocarbons [9, 10] makes them ideal candidates for use in hydrogen production. Hydrocarbons can be converted into hydrogen with by-products of water, carbon dioxide, and trace amounts of carbon monoxide [9, 10]. However, the platinum catalyst of a proton-exchange membrane fuel cell has little tolerance to carbon monoxide [11, 12] and thus a preferential oxidation process is often required [13, 14], which presents a significant design problem. Such procedures add to the complexity, size, parasitic power drain, and overall cost of a fuel cell, which will create structural design problems. Consequently, it is desirable to use methanol as the source of hydrogen for a fuel cell, thereby yielding a reformate gas

comprising primarily hydrogen and carbon dioxide [5, 6]. The reformate stream may contain a sufficiently low concentration of carbon monoxide and sufficiently pure hydrogen gas to be used for a desired application [15, 16]. Advantageously, the reaction can occur at a temperature far less than that needed for hydrocarbons.

The use of microchannel reactors as a methanol processor for hydrogen production will be inherently advantageous due to enhanced heat and mass transfer [17, 18]. However, there are many design challenges involved in practically realizing a microchannel reactor for fuel cell applications. For example, high catalyst loadings required to achieve the desired conversions, optimum shapes required to ensure low pressure drops, and enhanced ability of mixing to improve mass transfer must be achieved simultaneously. Experimentally, novel reactor design methods have been suggested with the use of micromachining techniques, such as deep-reactive ion etching [19, 20], electrochemical discharge machining [21], and sacrificing templates [22], to address these challenges. Numerically, computational fluid dynamics has been used to solve problems that include heat transfer and fluid flow [23, 24], and their solutions will enable the design and manufacture of improved reactors [25, 26]. Advantageously, the structure can be shaped to fit the reaction region into which it is to be disposed, for example, V-shaped or U-shaped reactors [27], T-shaped reactors [28], catalytic plate reactors [29], capillary reactors [30]. The reactors can be of any other configuration or shape as required by process intensification. Unfortunately, the results do not easily extend to the optimization or design principles of complex structured reactor systems. Furthermore, the causes of the transport phenomena of protruded reactors, on which very little in-depth research has been conducted, are still incompletely understood. Consequently, there remains a need for fundamental studies on the physics of processes involving heat and mass transfer and their coupling with fluid flow.

The present study focuses upon the physics of heat and mass transfer processes in a protruded millisecond microchannel reactor, wherein a steam reforming reaction is proceeding and protrusions are used to improve the transport processes involved. Parametric analysis of the reactor system is carried out using a three-dimensional numerical model that is sufficiently detailed to delineate the role of geometric features and operation conditions in reactor performance. Computational fluid dynamics analyses are performed under different sets of circumstances. In analysing the mechanisms involved in the intensified processes, account is taken of the factors that may influence the reactor performance. New insights into the physics of the processes are presented, with recommendations on how to optimize reactor design for better performance. The present study aims to understand the causes of the phenomena of process intensification in a protruded millisecond microchannel reactor. Particular emphasis is placed on delineating the role of geometric features and operation conditions in reactor performance. The results have implications for hydrogen production and beyond, for example, for the study of transport phenomena in microchannel reactors with a complicated structure.

2. Reactor system

Today most syngas is generated via thermal conversion of hydrocarbon, particularly by steam reforming of methane or by partial oxidation. The present study focuses upon the physics of heat and mass transfer processes in a protruded millisecond microchannel reactor, wherein a steam reforming reaction is proceeding and hemispherical protrusions are used to improve the transport processes involved. The chemical reaction proceeds to produce a hydrogen containing gas stream in the reactor with flat or protruded reforming channels. The structure of the protruded channel is illustrated schematically in Figure 1 with the hemispherical protrusions indicated. The structure of the flat channel is illustrated schematically in Figure 2 with the exothermic oxidation and endothermic reforming reactions indicated. The protruded channel comprises an array of hemispherical protrusions extending downstream from the inlet toward the outlet. The protrusions coated with the reformation catalyst are

1.0 mm in diameter, and the protrusions are 0.6 mm in diameter if they are uncoated. For the purposes of comparison and analysis, two types of sections through the channels are defined: the longitudinal section along the spherical centre and the longitudinal section along the spherical edge. The number of protrusions is adjusted while maintaining their spacing, if the channel length is changed.

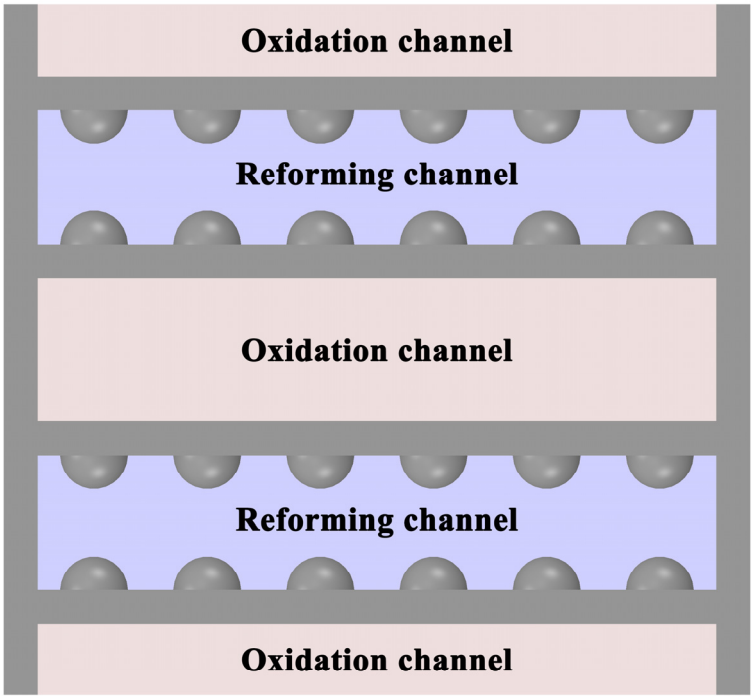

Figure 1. Illustration representation of the structure of the protruded channel where the protrusions are hemispherical in shape and arranged regularly on the wall surfaces.

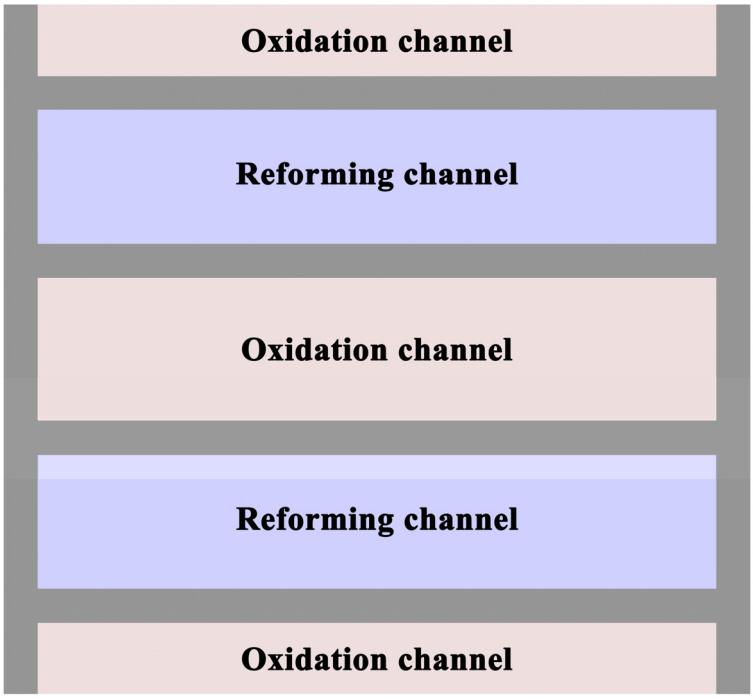

Figure 2. Illustration representation of the structure of the flat channel with the exothermic oxidation and endothermic reforming reactions indicated.

The channels are 60.0 mm in length, 5.6 mm in width, and 0.8 mm in height, the washcoat coatings are 0.20 mm in thickness, and the walls are 0.30 mm in thickness, unless otherwise expressly provided. The gaseous reactant mixture is supplied to the reactor in a molar ratio of steam to methanol of 150:100 or with an equivalence ratio of methanol to air of 0.8, unless otherwise specified. The reactor operates at one atmosphere pressure with an inlet temperature of 100 °C for both the gaseous reactant mixtures. The gaseous reactant mixtures are introduced respectively into the reactor with a free-stream velocity of 1.2 m/s at the oxidation channel inlet and a free-stream velocity of 4.0 m/s at the reforming channel inlet, unless otherwise noted.

3. Conservation equations

Fluid dynamics is concerned with the motion of fluids and the forces on them [31, 32]. Computational fluid dynamics refers to computation of the flow and forces using numerical analysis [33, 34]. A literal definition of computational fluid dynamics might therefore be the prediction of fluid motion and forces by computation using numerical analysis. Today, the term computational fluid dynamics is used to describe a broader range of calculations for a wide variety of scientific and engineering applications [35, 36]. Thermodynamics is an important consideration in many of these applications [37, 38]. It relates internal energy to temperature, which affects the flow of heat. Further sources of heat include thermal radiation and chemical reactions, in particular combustion [39, 40]. Heat transfer may involve conduction in solid materials, coupled with the fluid flow, known as conjugate heat transfer [41, 42]. A modern definition of computational fluid dynamics would be the prediction of fluid motion and forces by computation using numerical analysis, generally extended to include heat, thermodynamics, chemistry and solids.

Numerical analysis provides many methods and algorithms that are suitable for computational fluid dynamics [43, 44]. The methods include finite volume, finite element, and finite difference, which calculate the distributions of properties, for example, pressure, velocity and temperature, over regions of space which are usually fixed. Alternative methods attribute properties to particles represented by points in space, whose motions are calculated [45, 46]. The present study describes numerical methods to solve problems in fluid dynamics, up to and including heat and some basic thermodynamics.

The reactor model describes governing equations, namely conservation of mass, momentum and energy, and associated physical models, for example, for viscosity, heat conduction and thermodynamics. The equations describe fluid motion, forces and heat in time and three-dimensional space. The equations of fluid dynamics in computational fluid dynamics treat the fluid as a continuous medium, or continuum [47, 48]. The fluid has properties that vary from point to point and are continuous throughout the solution domain, and whose derivatives are also continuous. Pressure is an important property of a fluid. It describes the amount of force per unit surface area which acts on a surface, in the direction perpendicular to the surface. Pressure is a scalar that produces a force vector with direction normal to the surface. While pressure exerts a force on a surface, the fluid experiences a force which is compressive in nature. The majority of properties, for example, pressure, temperature, energy, density, and volume, can be represented by a single number, or scalar. A scalar field describes a scalar property, for example, pressure, which varies from point to point across some spatial domain. Point locations can be defined in any co-ordinate system of axes, and in any orientation. A scalar field is invariant, meaning the scalar values are the same irrespective of the co-ordinate system used.

Space and fields are described in a co-ordinate system with right-handed rectangular Cartesian axes. The heat flux requires temperature to be defined. The thermodynamic scale defines temperature as a measure of the average kinetic energy of random motions of particle constituents of matter. It provides an absolute measure of temperature that is independent of the choice of working substance and includes a zero point. The behaviour of the gases under typical working conditions is captured by

the ideal gas equation of state. The ideal gas equation originates from classical thermodynamics as a combination of empirical laws. Later, it is derived from first principles from both statistical thermodynamics and kinetic theory, with temperature representing average kinetic energy. The derivations assume that molecules have no volume, undergo purely elastic collisions and there are no inter-molecular forces. A scale of temperature defined by the ideal gas equation of state is exactly equivalent to the thermodynamic temperature scale.

Numerical methods are used to solve the problem due to the complexity of the geometry and flow regime, for example, hydrodynamic instabilities, which may lead to the formation of periodic wakes [49, 50]. In the walls and the washcoat coatings, the total energy remains constant

$$\frac{\partial}{\partial x}\left(\kappa_w \frac{\partial T}{\partial x}\right)+\frac{\partial}{\partial y}\left(\kappa_w \frac{\partial T}{\partial y}\right)+\frac{\partial}{\partial z}\left(\kappa_w \frac{\partial T}{\partial z}\right)=0, \tag{1}$$

$$\frac{\partial}{\partial x}\left(\kappa' \frac{\partial T}{\partial x}\right)+\frac{\partial}{\partial y}\left(\kappa' \frac{\partial T}{\partial y}\right)+\frac{\partial}{\partial z}\left(\kappa' \frac{\partial T}{\partial z}\right)=0, \tag{2}$$

$$\kappa' = \left(1-\varepsilon_p\right)\kappa_s + \varepsilon_p \kappa_g, \tag{3}$$

where κ_w is the wall thermal conductivity, T is the temperature, κ_s is the solid phase thermal conductivity, ε_p is the porosity, κ' is the effective thermal conductivity, and the subscripts x, y, and z denote coordinate variables.

In the gas phase, the law of conservation of momentum is applied and the equation of species conservation is solved

$$\begin{aligned}&\frac{\partial}{\partial x}\left[\mu\left(\frac{\partial u_x}{\partial x}+\frac{\partial u_x}{\partial x}\right)\right]+\frac{\partial}{\partial y}\left[\mu\left(\frac{\partial u_x}{\partial y}+\frac{\partial u_y}{\partial x}\right)\right]+\frac{\partial}{\partial z}\left[\mu\left(\frac{\partial u_x}{\partial z}+\frac{\partial u_z}{\partial x}\right)\right]\\&-\frac{\partial}{\partial x}\left[\frac{2}{3}\mu\left(\frac{\partial u_{xx}}{\partial x}+\frac{\partial u_{yx}}{\partial y}+\frac{\partial u_{zx}}{\partial z}\right)\right]-\frac{\partial p}{\partial x}=0\end{aligned}, \tag{4}$$

$$\begin{aligned}&\frac{\partial}{\partial x}\left[\mu\left(\frac{\partial u_y}{\partial x}+\frac{\partial u_x}{\partial y}\right)\right]+\frac{\partial}{\partial y}\left[\mu\left(\frac{\partial u_y}{\partial y}+\frac{\partial u_y}{\partial y}\right)\right]+\frac{\partial}{\partial z}\left[\mu\left(\frac{\partial u_y}{\partial z}+\frac{\partial u_z}{\partial y}\right)\right]\\&-\frac{\partial}{\partial y}\left[\frac{2}{3}\mu\left(\frac{\partial u_{xy}}{\partial x}+\frac{\partial u_{yy}}{\partial y}+\frac{\partial u_{zy}}{\partial z}\right)\right]-\frac{\partial p}{\partial y}=0\end{aligned}, \tag{5}$$

$$\begin{aligned}&\frac{\partial}{\partial x}\left[\mu\left(\frac{\partial u_z}{\partial x}+\frac{\partial u_x}{\partial z}\right)\right]+\frac{\partial}{\partial y}\left[\mu\left(\frac{\partial u_z}{\partial y}+\frac{\partial u_y}{\partial z}\right)\right]+\frac{\partial}{\partial z}\left[\mu\left(\frac{\partial u_z}{\partial z}+\frac{\partial u_z}{\partial z}\right)\right]\\&-\frac{\partial}{\partial z}\left[\frac{2}{3}\mu\left(\frac{\partial u_{xz}}{\partial x}+\frac{\partial u_{yz}}{\partial y}+\frac{\partial u_{zz}}{\partial z}\right)\right]-\frac{\partial p}{\partial z}=0\end{aligned}, \tag{6}$$

$$\frac{\partial\left(\rho u_x w_k\right)}{\partial x}+\frac{\partial\left(\rho u_y w_k\right)}{\partial y}+\frac{\partial\left(\rho u_z w_k\right)}{\partial z}+\frac{\partial}{\partial x}\left(\rho w_k V_{k,x}\right)+\frac{\partial}{\partial y}\left(\rho w_k V_{k,y}\right)+\frac{\partial}{\partial z}\left(\rho w_k V_{k,z}\right)=0, \tag{7}$$

$$\vec{V}_g = \left(\frac{D_g^T M_g}{\rho Y_g M'}\right)\vec{\nabla}\left(\ln T\right) - D_g^m \vec{\nabla}\left(\ln\left(\frac{Y_g M'}{M_g}\right)\right), \tag{8}$$

where D^T, D^m, M, M', $\vec{V}$, μ, w, ρ, and u are the thermal diffusion coefficient, molecular diffusion

coefficient, molecular weight, average molecular weight, diffusion velocity vector, dynamic viscosity, mass fraction, density, and velocity, respectively, and the subscripts *k* and *g* denote the gaseous mixture and gas-phase species, respectively.

The ideal gas equation of state is solved, the energy-conservation and mass-conservation principles are applied, and the specific heat capacity is described

$$p = \frac{\rho}{M'} RT \,, \tag{9}$$

$$h_k(T) = h_k(298.15\ \mathrm{K}) + \int_{298.15\ \mathrm{K}}^{T} c_{p,k}\, dT \,, \tag{10}$$

$$\begin{aligned} &\frac{\partial(\rho u_x h)}{\partial x} + \frac{\partial(\rho u_y h)}{\partial y} + \frac{\partial(\rho u_z h)}{\partial z} + \frac{\partial}{\partial x}\left(\rho \sum_{k=1}^{\gamma} w_k h_k V_{k,x} - \kappa_g \frac{\partial T}{\partial x}\right) + \frac{\partial}{\partial y}\left(\rho \sum_{k=1}^{\gamma} w_k h_k V_{k,y} - \kappa_g \frac{\partial T}{\partial y}\right) \\ &+ \frac{\partial}{\partial z}\left(\rho \sum_{k=1}^{\gamma} w_k h_k V_{k,z} - \kappa_g \frac{\partial T}{\partial z}\right) = 0 \end{aligned} \,, \tag{11}$$

$$\frac{\partial(\rho u_x)}{\partial x} + \frac{\partial(\rho u_y)}{\partial y} + \frac{\partial(\rho u_z)}{\partial z} = 0 \,, \tag{12}$$

wherein γ denotes the total number of gas-phase species, and R, h, c_p, and κ are the ideal gas constant, enthalpy, specific heat capacity at constant pressure, and thermal conductivity, respectively.

On the washcoat coating surface, the equation of species coverage is of the form

$$\frac{\theta_m \dot{r}_m}{\Gamma} = 0 \,, \quad m = 1, \ldots, \gamma' \,, \tag{13}$$

where the subscript m denotes the surface species, and Γ, γ', and θ is the site density, total number of surface species, and coverage, respectively.

The effective gaseous diffusivity can be expressed in the form

$$\frac{1}{D_i'} = \frac{\tau_p}{\varepsilon_p}\left(\frac{1}{D_i^K} + \frac{1}{D_i^m}\right), \tag{14}$$

$$D_i^K = \frac{d}{3}(8RT)^{0.5}(\pi W_i)^{-0.5}, \tag{15}$$

where D^K, D', d, ε_p, and τ_p are the Knudsen diffusion coefficient, effective gaseous diffusion coefficient, average pore diameter, porosity, and tortuosity, respectively.

At the fluid-coating interfaces, the equation of gas-phase species conservation is solved and the conservation-of-energy principle is applied

$$\eta\lambda M_k (\dot{r}_k)_\Theta + \left(\rho w_k V_{k,y \text{ or } z}\right)_\Theta = 0, \ k = 1, \ldots, K_g \,. \tag{16}$$

$$\kappa'\left(\frac{\partial T}{\partial y}\right)_{\Omega+} - \kappa_g\left(\frac{\partial T}{\partial y}\right)_{\Omega-} + \kappa'\left(\frac{\partial T}{\partial z}\right)_{\Omega+} - \kappa_g\left(\frac{\partial T}{\partial z}\right)_{\Omega-} + \sum_{k=1}^{K_g}(\dot{r}_k h_k W_k)_\Omega = 0 \,. \tag{17}$$

where η and λ is the effectiveness factor and surface area factor, and the subscript Θ denotes the fluid-coating interface.

4. Results and discussion

4.1. Effect of inlet velocity

Computational fluid dynamics analyses are carried out under different inlet velocity conditions. In analysing the intensification mechanisms involved, account is taken of the factors that may influence

the reactor performance. The effect of inlet velocity is investigated to understand how to improve the efficiency and performance of the reactor.

Calculations are performed under varying flow conditions, and the results are presented in Figure 3 with two-dimensional contour maps of temperature in the reactor. Accordingly, the two-dimensional contour maps of hydrogen mole fraction in the reactor are presented in Figure 4 under different inlet velocity conditions. The study is directed to varying the inlet velocity of the reforming process flow stream while maintaining a constant inlet velocity of the oxidant containing gas stream. The inlet velocity of the process flow stream is determinative of to what degree and when the endothermic reforming reaction occurs in the reactor. The overall temperature can be controlled based on the inlet velocity. As the inlet velocity increases from 4.0 m/s to 9.0 m/s, the maximum temperature is increased from 260 °C to 340 °C. While the inlet velocity affects the temperature greatly, the hydrogen mole fraction at the reactor outlet does vary substantially. As the inlet velocity is increased, the endothermic reforming reaction front shifts downstream. Advantageously, the inlet velocity of the reforming process flow stream matches that of the surrounding oxidation channel flow stream while maximizing mass transfer of the reactants of the fluid to the washcoat coating surface. However, the rate of diffusion of gas-phase species to the washcoat coating surface is determined by the gradient of species concentration and the height of the channels. Consequently, the methanol concentration and the channel height can be chosen so that the rate of delivery of the fuel to the washcoat coating surface is not diffusion limited and reaches a value high enough to maximize the conversion of methanol to hydrogen to a desired level. Alternatively, the reforming channels are designed in a protruded manner such that methanol can be effectively converted to hydrogen due to the successive continuous interruptions in the presence of hemispherical protrusions, and thus the product concentration is very high around the protruded regions. Accordingly, performance comparisons between the flat and protruded designs may be needed to further illustrate the effect of inlet velocity.

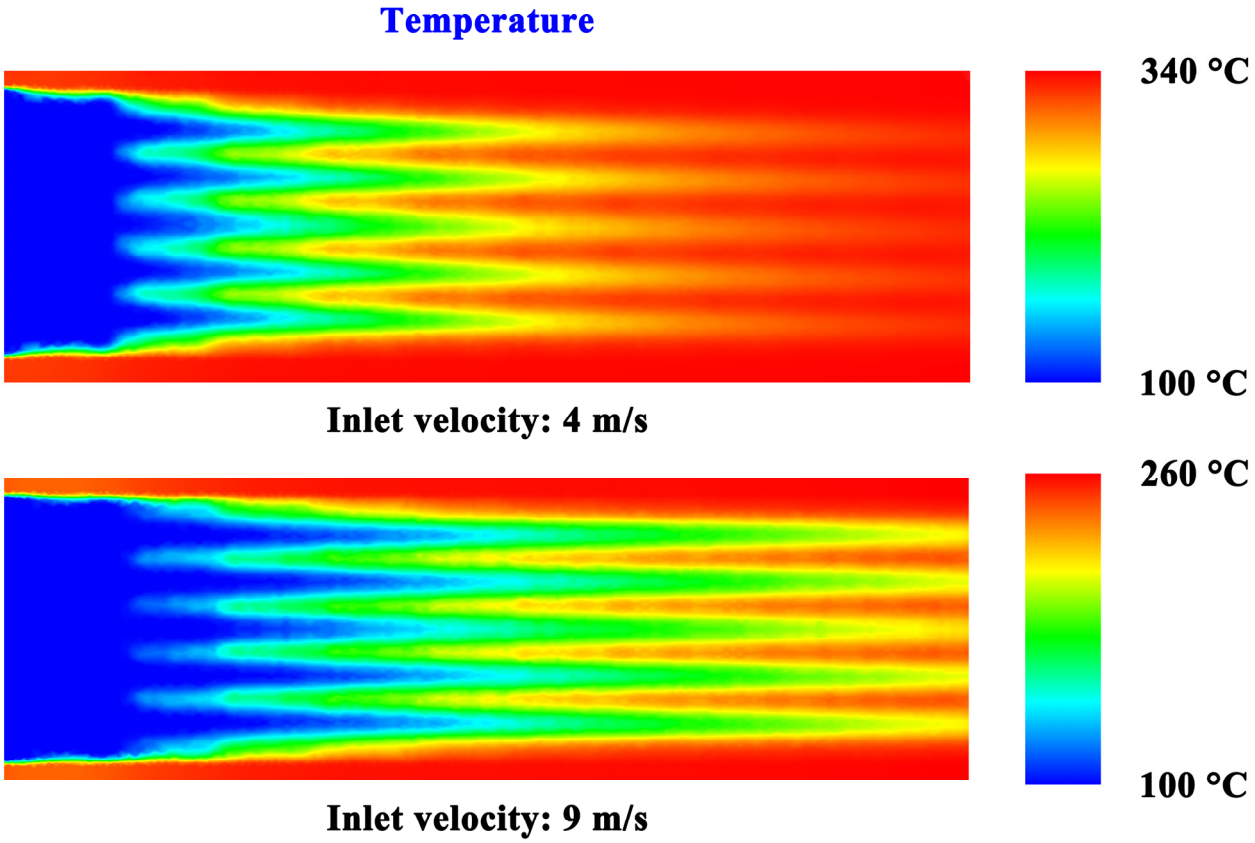

Figure 3. Two-dimensional contour maps of temperature in the protruded millisecond microchannel reactor under different inlet velocity conditions.

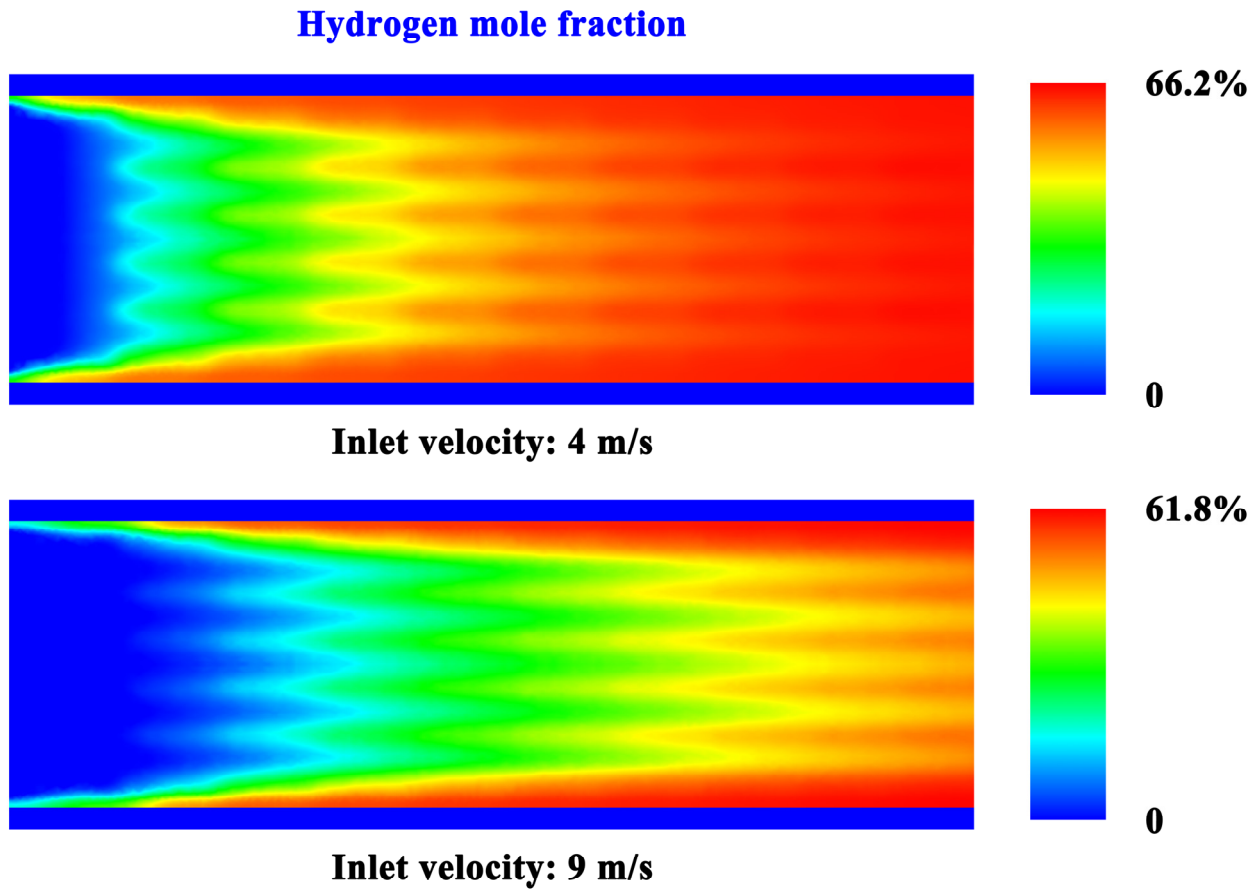

Figure 4. Two-dimensional contour maps of hydrogen mole fraction in the protruded millisecond microchannel reactor under different inlet velocity conditions.

The two-dimensional contour maps of hydrogen mole fraction in a longitudinal section along the spherical centre are illustrated in Figure 5 with the hemisphere location indicated. At the washcoat coating surface, the protruded channel inherently has a stationary layer of the fluid through which the transferred heat must pass, which is referred to as a velocity boundary layer. The protrusions can be properly positioned within the channels to interrupt the smooth flow of the fluid at appropriate intervals in a way that the thickness of boundary layer can be reduced effectively. However, the interruptions must be continued. Successive continuous interruptions are achieved in the flow of the fluid in the protruded channels. Accordingly, methanol can be converted effectively to hydrogen due to the successive continuous interruptions in the presence of hemispherical protrusions.

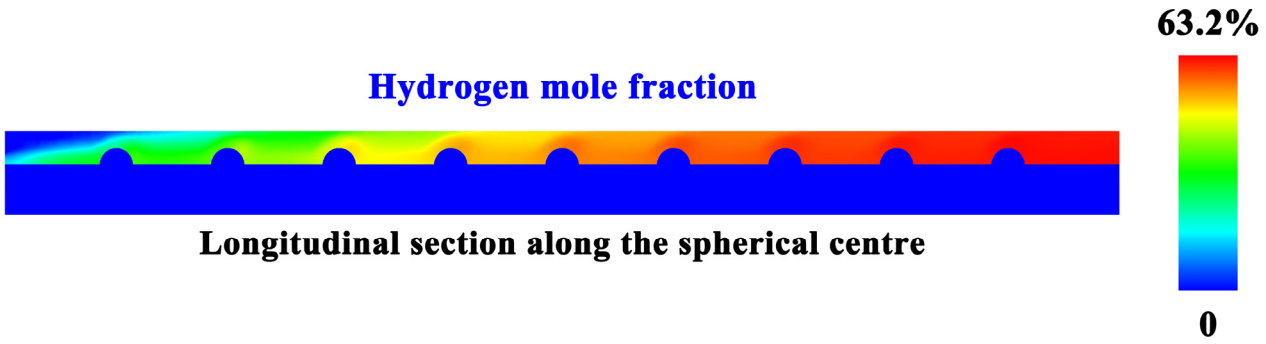

Figure 5. Two-dimensional contour maps of hydrogen mole fraction in a longitudinal section along the spherical centre.

The two-dimensional contour maps of temperature on the washcoat coating surface in the reactor are illustrated in Figure 6 with the reforming channel indicated. Accordingly, the two-dimensional contour maps of velocity on the washcoat coating surface in the reactor are illustrated in Figure 7 with

the reforming channel indicated. The temperatures are sufficient for reforming duty. In particular, the temperatures of the protrusions are relatively high and thus the endothermic reforming reaction is favoured. Heat is transferred rapidly into the protruded channel due to its very small dimension in the normal direction, while the gradients of temperature in the spanwise direction remain sufficiently constant. The velocity of flow of the fluid flowing in the bulk stream around or surrounding the protrusion while the reaction is proceeding is much higher than the velocity of flow of the stream in the vortex region, which will create an almost stationary region of higher residence time and therefore of higher conversion. On the other hand, the protruded design of the reactor provides a flow passage for the fluid comprising a succession of flow passage chamber portions separated from each other by intervening protrusion portions of smaller cross section, and thus of smaller flow capacity, transverse to the flow direction. Accordingly, the fluid travels through the reforming channel at a higher velocity in the protrusion portions than in the chamber portions. The fluid velocity in the protrusion portions is sufficiently high so that the thickness of the boundary layer on the washcoat coating surface can be effectively reduced, thereby facilitating the heat and mass transfer within the reactor.

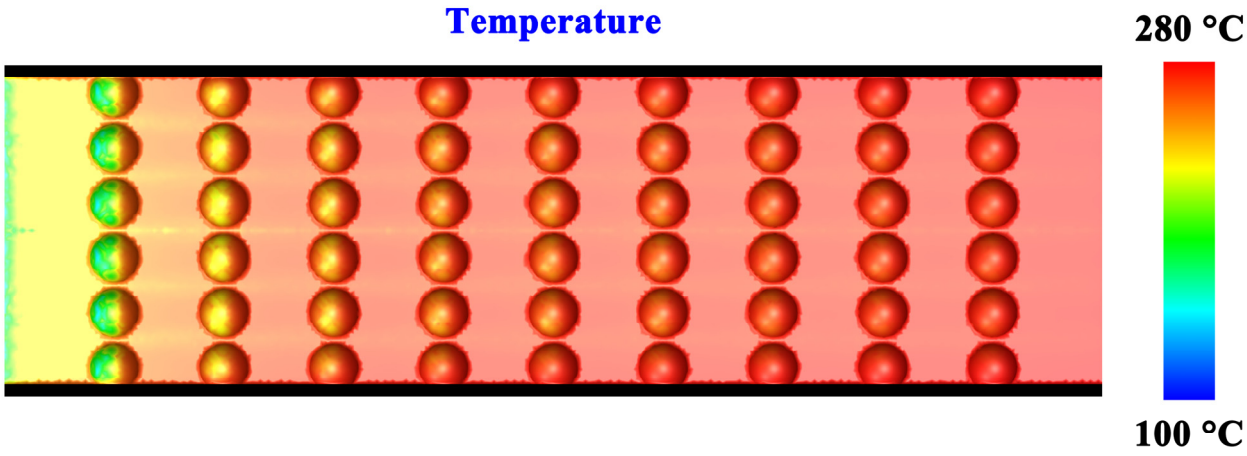

Figure 6. Two-dimensional contour maps of temperature on the washcoat coating surface in the reactor with the reforming channel indicated.

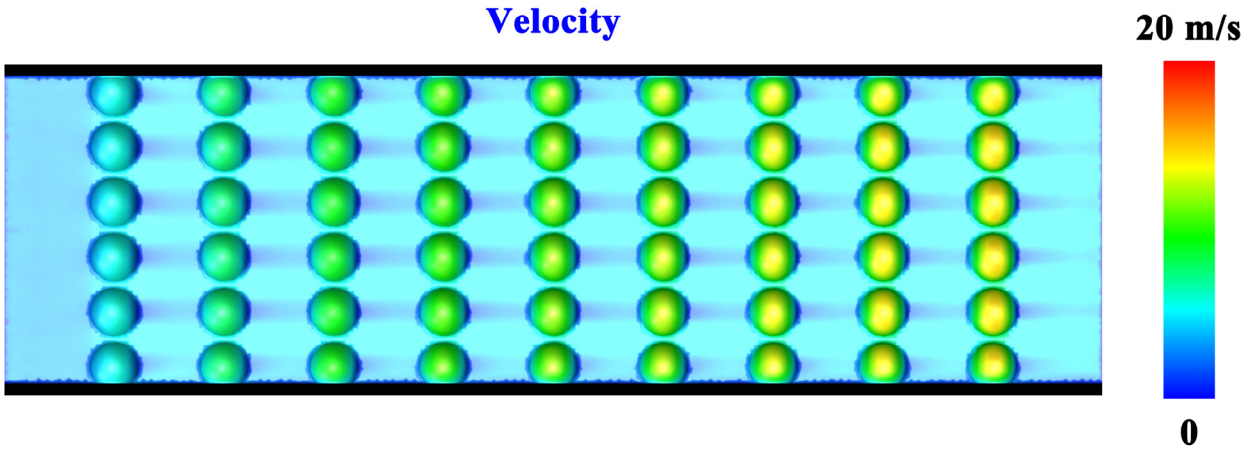

Figure 7. Two-dimensional contour maps of velocity on the washcoat coating surface in the reactor with the reforming channel indicated.

4.2. Effect of steam-to-methanol molar ratio

The effect of the molar ratio of steam to methanol on the methanol conversion and hydrogen productivity is evaluated, and the results for the flat channel and for the protruded are presented in Figure 8 in which the hydrogen productivity is calculated per channel. At a higher steam-methanol ratio, efficient conversion is possible, as the reactants undergo reforming in the reactor to a greater extent.

However, the rate at which hydrogen is produced is lower, as the amount of heat that is released by the oxidation reaction is in an excess of requirements. A more efficient process is desired, since there is not necessarily a need for such excess energy. Additionally, the reformed gas leaving the reactor has a relatively low hydrogen content due to an excess of steam. At a lower steam-methanol ratio, the conversion is relatively low, the oxidation reaction releases less heat than is required. However, the hydrogen productivity can be maintained at a sufficiently high level. This is not always advantageous, as only part of methanol is converted to hydrogen. Protrusions can be used to improve the conversion and productivity due to enhanced heat and mass transfer, as they behave as a baffle to direct flow of the reforming process flow stream. The rates of heat and mass transfer may be partially controlled by the diameter and position of each protrusion coupled to the surface of the wall, and thus the reaction may be driven toward the production of hydrogen-rich gas.

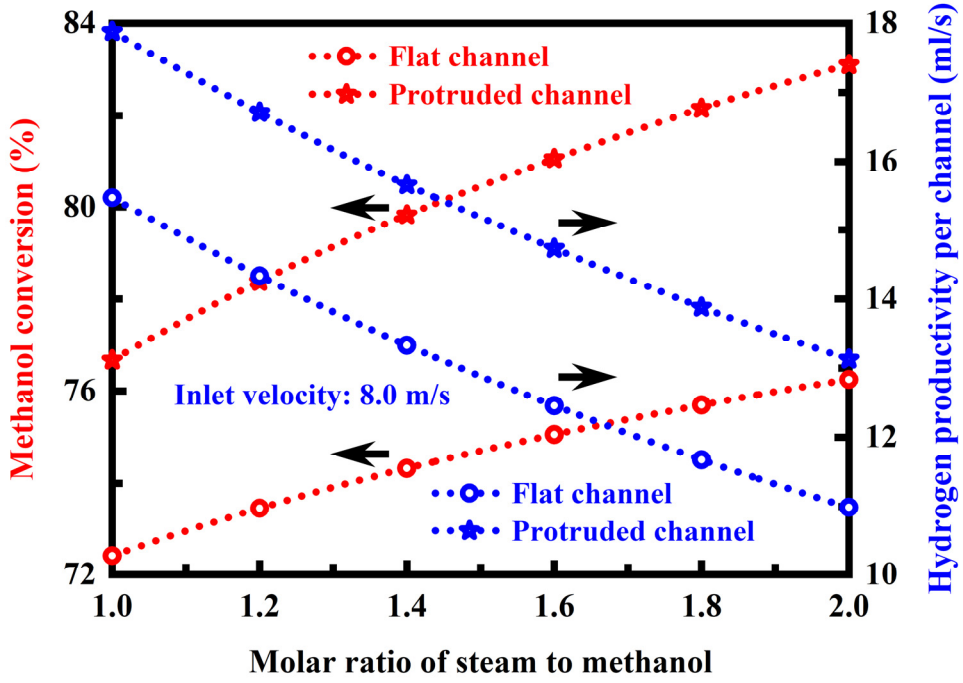

Figure 8. Effects of the molar ratio of steam to methanol on the methanol conversion and the hydrogen productivity per channel.

The effect of the molar ratio of steam to methanol on the temperature along the washcoat coating centreline is illustrated in Figure 9 for the flat channel and for the protruded channel under otherwise identical conditions. Necessary adjustments to the feed compositions, for example, the steam-methanol ratio, can be made to control the maximum reactor temperature within certain needed limits. In the reforming process, it is essential that the temperature at which the reaction proceeds is critical for successful optimum operation [51, 52]. Consequently, it is important to maintain the temperature within a specific range, which is very narrow, for example, in the range from 200 °C to 300 °C. A variation in the temperature outside this range causes undesired side reactions to take place and may deactivate the catalytically-active components [51, 52], which reduces the hydrogen productivity of the reactor and therefore causes the performance to degrade. This is the case for the flat channel, since the reactants are raised to temperatures in excess of 300 °C at a higher steam-methanol ratio, at which the protruded channel is of sufficiently low temperatures for the reaction to occur. Accordingly, the flat channel has a smaller hydrogen concentration at the reactor outlet than the protruded channels. The temperature along the washcoat coating centreline depends upon the steam-methanol ratio. There is a positive correlation between the temperature and the steam-methanol ratio. At a higher steam-methanol ratio, the amount of heat that is released may be in excess of requirements, for example, in the case of the flat channel. In this case, the temperature is high and therefore rapid formation of hydrogen is possible. However, the

disadvantage gained by a higher steam-methanol ratio is that the hydrogen concentration at the reactor outlet is low. A moderate steam-methanol ratio is desired, since there is not necessarily a need for excess energy. The advantage gained by a lower steam-methanol ratio is that the hydrogen concentration at the reactor outlet is high. However, the amount of heat that is released is less than the requirement, therefore enabling a lower, overall reaction temperature to be achieved in the reactor. Temperatures greater than 200 °C are often required in order to achieve practical conversion levels.

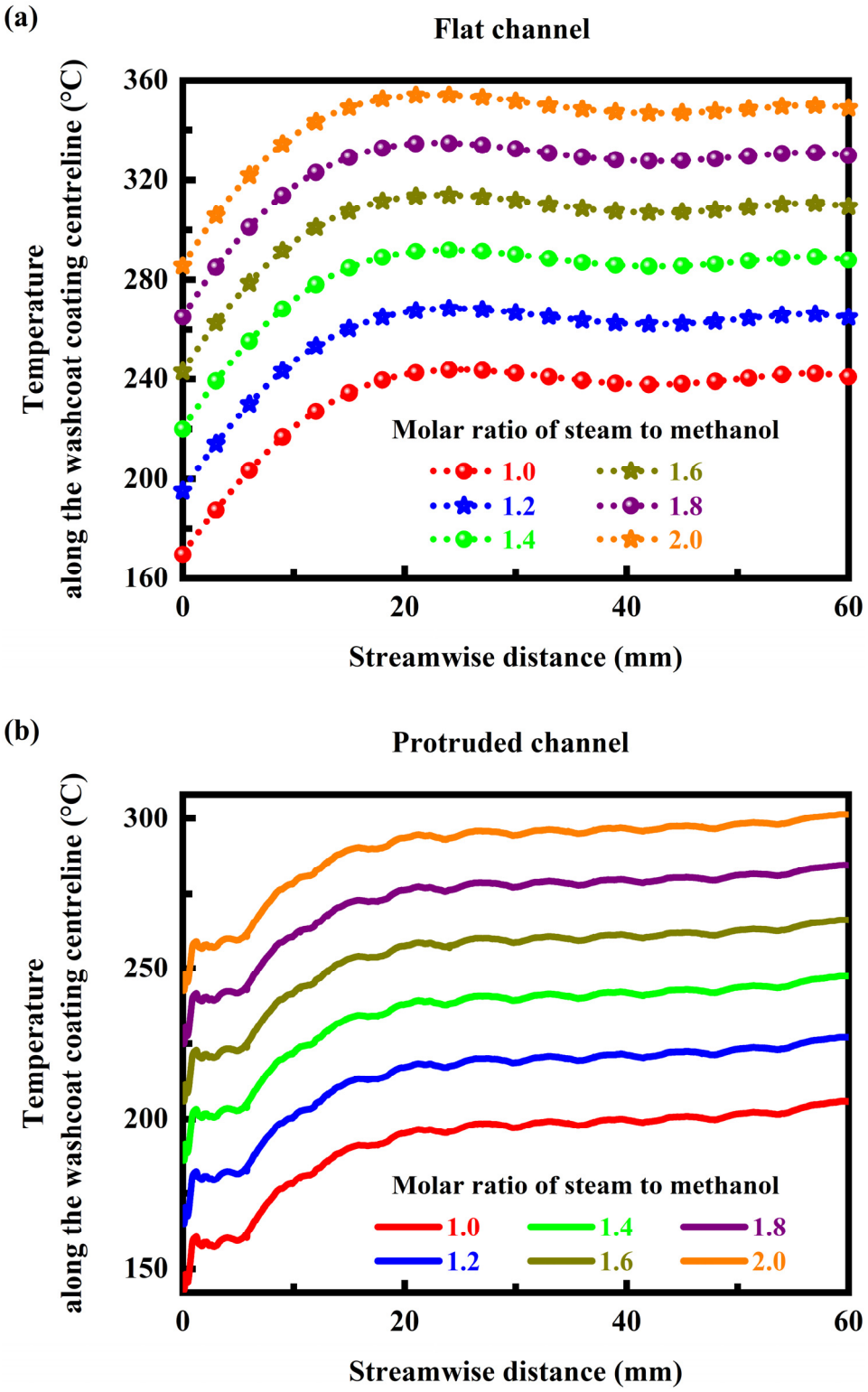

Figure 9. (a) Effect of the molar ratio of steam to methanol on the temperature along the washcoat coating centreline for the flat channel. (b) Effect of the molar ratio of steam to methanol on the temperature along the washcoat coating centreline for the protruded channel.

The hydrogen concentration profiles along the centreline of the flat channel and of the protruded channel are presented in Figure 10 at different molar ratios of steam to methanol. The flat channel has a smaller hydrogen concentration at the reactor outlet than the protruded channels, and the advantage gained by a lower steam-methanol ratio is that the hydrogen concentration at the reactor outlet is high. Without the heat supplied sufficiently by the oxidation reaction, the temperature is too low for sufficiently rapid formation of hydrogen or for steam reforming of methanol. The steam-methanol ratio may vary to obtain a desired hydrogen concentration at the reactor outlet. If the fuel cell is to be used to power a vehicle, the fuel cell, and the steam reformer used to supply hydrogen to the fuel cell, must be compact. The feed stream may be delivered to the steam reformer at an elevated temperature, and accordingly may provide at least a portion of the required heat. When a burner or other combustion chamber is used, a fuel stream is consumed and a heated exhaust stream is produced. The feed stream is vaporized prior to undergoing the reforming reaction, and a heating assembly may be adapted to heat and vaporize any liquid components of feed stream. Methanol is a particularly well-suited carbon-containing feedstock for steam reforming reactions. Methanol steam reforming typically takes place at a lower temperature than when other carbon-containing feedstocks are reformed. Hydrogen gas will be the majority, or primary, component of the reformate stream. Although the reformate stream contains a substantial amount of hydrogen gas, the stream may also be referred to as a mixed gas stream because it also contains gases other than hydrogen gas. Examples of these gases include carbon dioxide, carbon monoxide, water, methane or unreacted methanol or other carbon-containing feedstocks [53, 54]. The reformate stream may contain sufficiently pure hydrogen gas or sufficiently low concentrations of the non-hydrogen components to be used for a desired application. In such a situation, the product hydrogen stream may be formed directly from the reformate stream. However, many applications require hydrogen gas that has greater purity or a reduced concentration of one or more non-hydrogen components that is present in reformate stream [55, 56]. Therefore, the steam reformer may, but is not required to, include a separation region in which the hydrogen purity of the reformate stream is increased or the concentration of at least one non-hydrogen component is reduced. The hydrogen-rich stream has a greater concentration of hydrogen gas than the reformate stream or has a reduced concentration of at least one non-hydrogen component of the reformate stream.

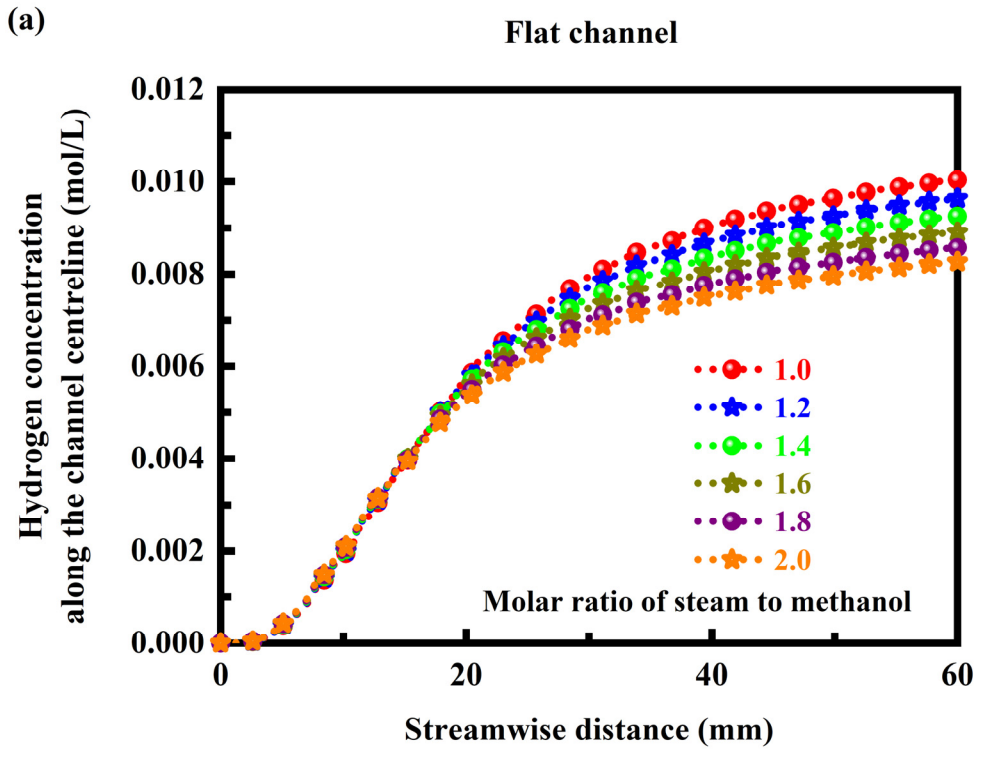

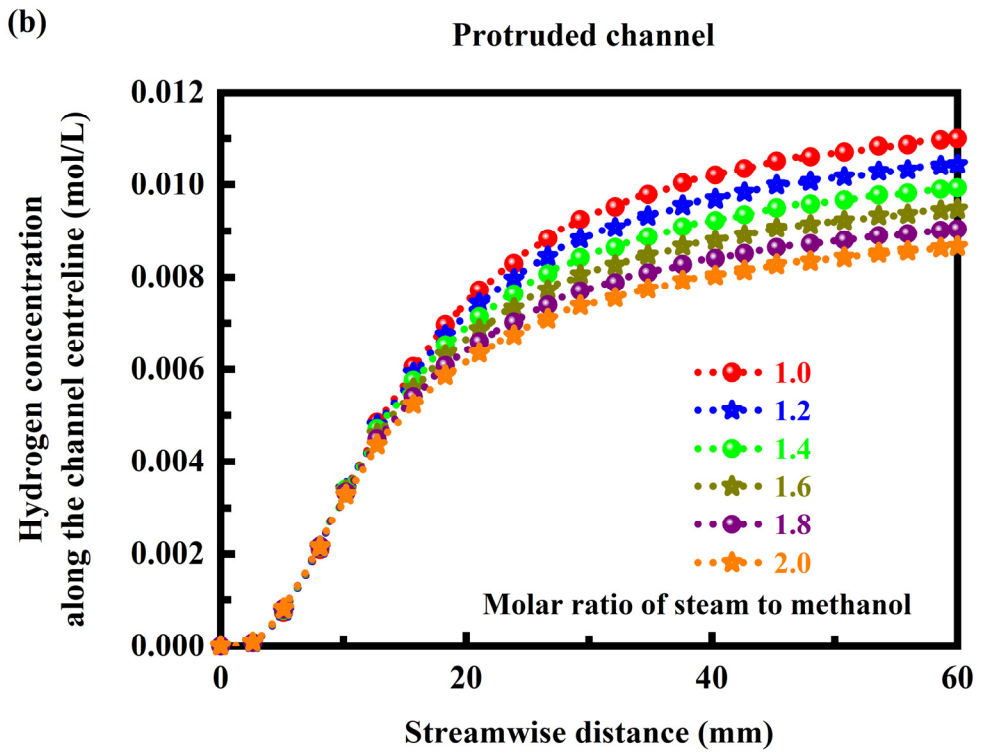

Figure 10. (a) Effect of the molar ratio of steam to methanol on the hydrogen concentration along the centreline of the flat channel. (b) Effect of the molar ratio of steam to methanol on the hydrogen concentration along the centreline of the protruded channel.

5. Conclusions

Computational fluid dynamics is used to delineate the role of geometric features and operation conditions in the performance of a millisecond microchannel reforming reactor. The effects of inlet velocity and steam-to-methanol ratio were investigated to understand how to improve the efficiency and performance of the reactor. The conclusions are summarized primarily as follows:

- The flow rates and steam-to-methanol ratio must be closely adjusted to satisfy the reaction conditions in practice, thereby ensuring efficient operation of the reactor, such as improved hydrogen production and reduced pressure drops.
- Protrusions are very effective in improving the transport processes involved without greatly impairing hydraulic performance, and high conversions and good yields can be obtained with only milliseconds residence of the mixtures within the reactor.
- Advantageously, the inlet velocity of the reforming process flow stream matches that of the surrounding oxidation channel flow stream while maximizing mass transfer of the reactants of the fluid to the washcoat coating surface.
- The protrusions can be properly positioned within the channels to interrupt the smooth flow of the fluid at appropriate intervals in a way that the thickness of boundary layer can be reduced effectively.
- Methanol can be converted effectively to hydrogen due to the successive continuous interruptions in the presence of hemispherical protrusions.
- The fluid velocity in the protrusion portions is sufficiently high so that the thickness of the boundary layer on the washcoat coating surface can be effectively reduced, thereby facilitating the heat and mass transfer within the reactor.
- Necessary adjustments to the molar ratio of steam to methanol can be made to control the maximum reactor temperature within certain needed limits.

- Protrusions can be used to improve the conversion and productivity due to enhanced heat and mass transfer, as they behave as a baffle to direct flow of the reforming process flow stream.

References

[1] T. Hos, G. Sror, and M. Herskowitz. Autothermal reforming of methanol for on-board hydrogen production in marine vehicles. *International Journal of Hydrogen Energy*, Volume 49, Part A, 2024, Pages 1121-1132.

[2] H.E. Figen and S.Z. Baykara. Hydrogen production by partial oxidation of methane over Co based, Ni and Ru monolithic catalysts. *International Journal of Hydrogen Energy*, Volume 40, Issue 24, 2015, Pages 7439-7451.

[3] D. Pashchenko. Performance evaluation of a combined power generation system integrated with thermochemical exhaust heat recuperation based on steam methane reforming. *International Journal of Hydrogen Energy*, Volume 48, Issue 15, 2023, Pages 5823-5835.

[4] D. Pashchenko, R. Mustafin, and I. Karpilov. Thermochemical recuperation by steam methane reforming as an efficient alternative to steam injection in the gas turbines. *Energy*, Volume 258, 2022, Article Number: 124913.

[5] J.D. Holladay, Y. Wang, and E. Jones. Review of developments in portable hydrogen production using microreactor technology. *Chemical Reviews*, Volume 104, Issue 10, 2004, Pages 4767-4790.

[6] D.R. Palo, R.A. Dagle, and J.D. Holladay. Methanol steam reforming for hydrogen production. *Chemical Reviews*, Volume 107, Issue 10, 2007, Pages 3992-4021.

[7] Z. Su, J. Guan, Y. Liu, D. Shi, Q. Wu, K. Chen, Y. Zhang, and H. Li. Research progress of ruthenium-based catalysts for hydrogen production from ammonia decomposition. *International Journal of Hydrogen Energy*, Volume 51, Part B, 2024, Pages 1019-1043.

[8] J. Jang and M. Han. Ammonia autothermal reformer with air side-stream distribution for hydrogen production. *International Journal of Hydrogen Energy*, Volume 49, Part B, 2024, Pages 1468-1481.

[9] A.A. Levikhin and A.A. Boryaev. High-temperature reactor for hydrogen production by partial oxidation of hydrocarbons. *International Journal of Hydrogen Energy*, Volume 48, Issue 72, 2023, Pages 28187-28204.

[10] D. Pashchenko. Intra-particle diffusion limitation for steam methane reforming over a Ni-based catalyst. *Fuel*, Volume 353, 2023, Article Number: 129205.

[11] K. Darowicki, L. Gawel, M. Mielniczek, A. Zielinski, E. Janicka, J. Hunger, and L. Jorissen. The impedance of hydrogen oxidation reaction in a proton exchange membrane fuel cell in the presence of carbon monoxide in hydrogen stream. *Applied Energy*, Volume 279, 2020, Article Number: 115868.

[12] V.F. Valdés-López, T. Mason, P.R. Shearing, and D.J.L. Brett. Carbon monoxide poisoning and mitigation strategies for polymer electrolyte membrane fuel cells - A review. *Progress in Energy and Combustion Science*, Volume 79, 2020, Article Number: 100842.

[13] Y. Xi and A. Heyden. Preferential oxidation of CO in hydrogen at nonmetal active sites with high activity and selectivity. *ACS Catalysis*, Volume 10, Issue 9, 2020, Pages 5362-5370.

[14] L. Zhong, M. Barreau, V. Caps, V. Papaefthimiou, M. Haevecker, D. Teschner, W. Baaziz, E. Borfecchia, L. Braglia, and S. Zafeiratos. Improving the catalytic performance of cobalt for CO preferential oxidation by stabilizing the active phase through vanadium promotion. *ACS Catalysis*, Volume 11, Issue 9, 2021, Pages 5369-5385.

[15] C.E. Taylor, B.H. Howard, and C.R. Myers. Methanol conversion for the production of hydrogen. *Industrial & Engineering Chemistry Research*, Volume 46, Issue 26, 2007, Pages 8906-8909.

[16] A.M. Ranjekar and G.D. Yadav. Steam reforming of methanol for hydrogen production: A critical analysis of catalysis, processes, and scope. *Industrial & Engineering Chemistry Research*, Volume 60, Issue 1, 2021, Pages 89-113.
[17] R.S. Wegeng, L.R. Pederson, W.E. TeGrotenhuis, and G.A. Whyatt. Compact fuel processors for fuel cell powered automobiles based on microchannel technology. *Fuel Cells Bulletin*, Volume 3, Issue 28, 2001, Pages 8-13.
[18] G. Kolb, S. Keller, M. O'Connell, S. Pecov, J. Schuerer, B. Spasova, D. Tiemann, and A. Ziogas. Microchannel fuel processors as a hydrogen source for fuel cells in distributed energy supply systems. *Energy & Fuels*, Volume 27, Issue 8, 2013, Pages 4395-4402.
[19] W.T. Pike, W.J. Karl, S. Kumar, S. Vijendran, and T. Semple. Analysis of sidewall quality in through-wafer deep reactive-ion etching. *Microelectronic Engineering*, Volumes 73-74, 2004, Pages 340-345.
[20] F. Marty, L. Rousseau, B. Saadany, B. Mercier, O. Français, Y. Mita, and T. Bourouina. Advanced etching of silicon based on deep reactive ion etching for silicon high aspect ratio microstructures and three-dimensional micro- and nanostructures. *Microelectronics Journal*, Volume 36, Issue 7, 2005, Pages 673-677.
[21] S. Ahmed, A. Speidel, J.W. Murray, N. Ahmed, M. Cuttell, and A.T. Clare. Electrolytic-dielectrics: A route to zero recast electrical discharge machining. *International Journal of Machine Tools and Manufacture*, Volume 181, 2022, Article Number: 103941.
[22] A. Lale, M. Schmidt, M.D. Mallmann, A.V.A. Bezerra, E.D. Acosta, R.A.F. Machado, U.B. Demirci, and S. Bernard. Polymer-derived ceramics with engineered mesoporosity: From design to application in catalysis. *Surface and Coatings Technology*, Volume 350, 2018, Pages 569-586.
[23] W.-L. Li, J.-H. Wang, H. Chen, L. Shao, G.-W. Chu, and Y. Xiang. CFD analysis on the intensified mechanism of gas-liquid mass transfer in a microporous tube-in-tube microchannel reactor. *International Journal of Heat and Mass Transfer*, Volume 182, 2022, Article Number: 121914.
[24] C. Cao, N. Zhang, X. Chen, and Y. Cheng. A comparative study of Rh and Ni coated microchannel reactor for steam methane reforming using CFD with detailed chemistry. *Chemical Engineering Science*, Volume 137, 2015, Pages 276-286.
[25] M. Wójcik, Ł. Szabłowski, and O. Dybiński. Comparison of mathematical models of steam methane reforming process for the needs of fuel cells. *International Journal of Hydrogen Energy*, Volume 52, Part A, 2024, Pages 965-982.
[26] D. Pashchenko, R. Mustafin, and A. Mustafina. Steam methane reforming in a microchannel reformer: Experiment, CFD-modelling and numerical study. *Energy*, Volume 237, 2021, Article Number: 121624.
[27] A. Stefanescu, A.C. van Veen, C. Mirodatos, J.C. Beziat, and E. Duval-Brunel. Wall coating optimization for microchannel reactors. *Catalysis Today*, Volume 125, Issues 1-2, 2007, Pages 16-23.
[28] I.M. Hsing, R. Srinivasan, M.P. Harold, K.F. Jensen, and M.A. Schmidt. Simulation of micromachined chemical reactors for heterogeneous partial oxidation reactions. *Chemical Engineering Science*, Volume 55, Issue 1, 2000, Pages 3-13.
[29] M. Zanfir and A. Gavriilidis. Catalytic combustion assisted methane steam reforming in a catalytic plate reactor. *Chemical Engineering Science*, Volume 58, Issue 17, 2003, Pages 3947-3960.
[30] G. Dummann, U. Quittmann, L. Gröschel, D.W. Agar, O. Wörz, and K. Morgenschweis. The capillary-microreactor: A new reactor concept for the intensification of heat and mass transfer in liquid-liquid reactions. *Catalysis Today*, Volumes 79-80, 2003, Pages 433-439.
[31] F. Bezzo, S. Macchietto, and C.C. Pantelides. A general framework for the integration of computational fluid dynamics and process simulation. *Computers & Chemical Engineering*,

Volume 24, Issues 2-7, 2000, Pages 653-658.
[32] E. Delnoij, J.A.M. Kuipers, and W.P.M. van Swaaij. Computational fluid dynamics applied to gas-liquid contactors. *Chemical Engineering Science*, Volume 52, Issues 21-22, 1997, Pages 3623-3638.
[33] M. Bistolfi, N. Mancini, and F. Podenzani. Computational fluid dynamics modelling of multiphase reactors. *Computer Aided Chemical Engineering*, Volume 8, 2000, Pages 379-384.
[34] R.S. Neve. Computational fluid dynamics analysis of diffuser performance in gas-powered jet pumps. *International Journal of Heat and Fluid Flow*, Volume 14, Issue 4, 1993, Pages 401-407.
[35] J.A.M. Kuipers and W.P.M. van Swaaij. Computational fluid dynamics applied to chemical reaction engineering. *Advances in Chemical Engineering*, Volume 24, 1998, Pages 227-328.
[36] B.H. Xu and A.B. Yu. Numerical simulation of the gas-solid flow in a fluidized bed by combining discrete particle method with computational fluid dynamics. *Chemical Engineering Science*, Volume 52, Issue 16, 1997, Pages 2785-2809.
[37] M. Ishida. Hierarchical structure of thermodynamics. *Applied Energy*, Volume 67, Issues 1-2, 2000, Pages 221-230.
[38] M. Ishida. The role and limitations of endoreversible thermodynamics. *Energy*, Volume 24, Issue 12, 1999, Pages 1009-1014.
[39] F. Battin-Leclerc, P.A. Glaude, V. Warth, R. Fournet, G. Scacchi, and G.M. Côme. Computer tools for modelling the chemical phenomena related to combustion. *Chemical Engineering Science*, Volume 55, Issue 15, 2000, Pages 2883-2893.
[40] C.T. Goralski Jr. and L.D. Schmidt. Modeling heterogeneous and homogeneous reactions in the high-temperature catalytic combustion of methane. *Chemical Engineering Science*, Volume 54, Issue 24, 1999, Pages 5791-5807.
[41] K.D. Cole. Conjugate heat transfer from a small heated strip. *International Journal of Heat and Mass Transfer*, Volume 40, Issue 11, 1997, Pages 2709-2719.
[42] H.D. Nguyen, S. Paik, and J.N. Chung. Unsteady mixed convection heat transfer from a solid sphere: The conjugate problem. *International Journal of Heat and Mass Transfer*, Volume 36, Issue 18, 1993, Pages 4443-4453.
[43] E. Krause. Computational fluid dynamics: Its present status and future direction. *Computers & Fluids*, Volume 13, Issue 3, 1985, Pages 239-269.
[44] J.H. Adlam. Computation of two-dimensional time-dependent natural convection in a cavity where there are internal bodies. *Computers & Fluids*, Volume 14, Issue 2, 1986, Pages 141-157.
[45] M. Castro-Delgado and I. Celik. Analysis of free-surface flows past overflow gates using finite element method. *Computers & Fluids*, Volume 14, Issue 2, 1986, Pages 159-169.
[46] E. Turkel. Progress in computational physics. *Computers & Fluids*, Volume 11, Issue 2, 1983, Pages 121-144.
[47] B.H. Gilding. A numerical grid generation technique. *Computers & Fluids*, Volume 16, Issue 1, 1988, Pages 47-58.
[48] S.-W. Kim. A fine grid finite element computation of two-dimensional high Reynolds number flows. *Computers & Fluids*, Volume 16, Issue 4, 1988, Pages 429-444.
[49] R. López-Ruiz and Y. Pomeau. Transition between two oscillation modes. *Physical Review E*, Volume 55, Issue 4, 1997, Article Number: R3820(R).
[50] S. Piedra, E. Ramos, and J.R. Herrera. Dynamics of two-dimensional bubbles. *Physical Review E*, Volume 91, Issue 6, 2015, Article Number: 063013.
[51] D.L. Trimm. Catalysts for the control of coking during steam reforming. *Catalysis Today*, Volume 49, Issues 1-3, 1999, Pages 3-10.
[52] D.L. Trimm. Coke formation and minimisation during steam reforming reactions. *Catalysis Today*,

Volume 37, Issue 3, 1997, Pages 233-238.
[53] N. Takezawa, H. Kobayashi, A. Hirose, M. Shimokawabe, and K. Takahashi. Steam reforming of methanol on copper-silica catalysts; effect of copper loading and calcination temperature on the reaction. *Applied Catalysis*, Volume 4, Issue 2, 1982, Pages 127-134.
[54] P. Münster and H.J. Grabke. Kinetics of the steam reforming of methane with iron, nickel, and iron-nickel alloys as catalysts. *Journal of Catalysis*, Volume 72, Issue 2, 1981, Pages 279-287.
[55] S. Srinivasan, E.A. Ticianelli, C.R. Derouin, and A. Redondo. Advances in solid polymer electrolyte fuel cell technology with low platinum loading electrodes. *Journal of Power Sources*, Volume 22, Issues 3-4, 1988, Pages 359-375.
[56] D. Jansen and M. Mozaffarian. Advanced fuel cell energy conversion systems. *Energy Conversion and Management*, Volume 38, Issues 10-13, 1997, Pages 957-967.